# Comparison of various interpretation methods of the electric probe measurements in inductively coupled Ar and $O_2$ plasmas

Min Woo Seo, Min Keun Bae, and T. H. Chung[a)]
*Department of Physics, Dong-A University, Busan 604-714, South Korea*

(Received 12 January 2014; accepted 20 February 2014; published online 28 February 2014)

In low-pressure inductively coupled argon and oxygen discharges, the plasma density and electron temperature and the electron energy distribution function (EEDF) were obtained by using a cylindrical electric probe. The plasma densities were determined by various methods to interpret the probe current-voltage characteristic curve: the EEDF integration, the electron saturation current, the ion current at the floating potential, and the orbital-motion-limited (OML) ion current. Quite a good agreement exists between the plasma densities determined by various classical methods. Although the probe technique has some limitation in electronegative plasmas, the plasma densities determined from OML theory compare well with those measured by the ion saturation current at the floating potential in the oxygen discharges. In addition, the EEDFs of inductively coupled Ar and oxygen plasmas are observed to be nearly Maxwellian at the pressure range of 1-40 mTorr. © *2014 AIP Publishing LLC*. [http://dx.doi.org/10.1063/1.4867350]

## I. INTRODUCTION

The development of simple and reliable plasma diagnostics is essential for understanding plasma properties and further development of plasma technology. In plasma processing, plasma parameters such as the electron temperature and plasma density play a critical role. Number density, flux, and bombardment energy of positive ions affect the physical process. Electron energy distribution function (EEDF) governs the generation and transport of plasma species. For these reasons, the measurement of the plasma parameter such as the plasma density, electron temperature, and EEDF has been extensively studied.[1–6]

Electric probe is a non-invasive and convenient technique to diagnose a variety of plasmas. Cylindrical electric probes are used often because of their simplicity of construction and because planar probes, for example, are more perturbing to their local environment.[7] Simple cylindrical Langmuir probes are currently the main contact diagnostic tool for measuring plasma parameters in weakly ionized, low-pressure plasmas in both applied and basic plasma research. However, the interpretation of the measurements for even this simple case can be intricate and confusing.[6]

This study is devoted to the determination of the plasma density utilizing the cylindrical probe measurement. The plasma density is generally determined using various methods to interpret the current-voltage (I-V) curve of the electric probe: (i) from the electron saturation (ES) current measured at the plasma potential, (ii) from the integration over the EEDF, and (iii) from the ion saturation current when the probe is negatively biased.[5] The competing ion current theories are orbital-motion limited (OML) and the radial-motion theories.[8–10] However, use of radial-motion theories requires numerical solutions of Poisson's equation modelled to the experimentally measured probe characteristics, usually by iteration to obtain the temperature and density for the particular theory chosen.[9] These solutions are then plotted together with the experimental data and the closeness of the fit examined.

In the low density regime, it is common practice in the industry to use the OML theory of ion collection. This theory can be applied successfully well outside its intended range, but its error may be greatly enhanced at high densities.[10] Chen *et al*. have found an easier way to estimate the plasma density from the determination of the ion current at the floating potential by extrapolating based on the Child-Langmuir (CL) sheath law.[11]

Inductively coupled Ar or oxygen discharges in low-pressure regime (1–40 mTorr) have been mainly utilized for many industrial-materials processing such as etching and deposition of thin films.[12–15] The determination of plasma parameters is a critical issue in the control of plasma processing. In this work, probe measurements are performed in inductively coupled Ar and $O_2$ discharges with varying operating pressure. Among the various methods aforementioned, four methods (EEDF, ES, CL, and OML) are considered to obtain the plasma density. Comparisons will be made between the plasma densities measured by these versatile classical methods to interpret the probe I-V data. In addition, some discussions are given to EEDFs of low-pressure Ar and oxygen inductively coupled plasma (ICP) discharges.

## II. EXPERIMENTS AND INTERPRETATION METHODS

The plasma generation chamber consists of a stainless steel cylinder with a diameter 28 cm and a length of 30 cm. A 1.9 cm thick by 27 cm diameter tempered glass plate mounted on the one end separates the planar one-turn induction coil from the plasma. The induction coil is made of copper (with water-cooling) and connected to an L-type capacitive matching network and a rf power generator. The details of the apparatus are found in Ref. 16.

[a)]Electronic address: thchung@dau.ac.kr

 

The plasma chamber is evacuated by a diffusion pump, backed by a rotary pump, giving a base pressure of $9 \times 10^{-6}$ Torr. The operating gas pressure is controlled by adjusting the mass flow controller. The gas pressure is varied in the range of 1–40 mTorr. And a 13.56 MHz generator with a power output of 500 W drives rf current in a flat one-turn coil through the rf power generator and matching network. An rf-compensated cylindrical single electric probe was mounted through one of the ports on the vacuum chamber. The probe tip made of tungsten with a diameter of 0.1 mm and a length of 10 mm is used to measure the plasma parameters. The probe tip was located on the axis of the cylinder at 14 cm below the tempered glass plate. Probe circuit resistance is accounted for by the use of the reference ring probe with a resonance filter that reduces the rf distortion of probe characteristics.[2]

If the electrons are Maxwellian, the transition (exponential) region of the I-V curve should be represented as

$$I_e(V_{pr}) = n_e e A_p \left(\frac{kT_e}{2\pi m_e}\right)^{\frac{1}{2}} \exp\left(\frac{e(V_{pr} - V_p)}{kT_e}\right), \quad (1)$$

where $n_e$ is the electron density, $e$ is the electron charge, $A_p$ is the probe area, $T_e$ is the electron temperature, $k$ is the Boltzmann constant, $m_e$ is the mass of electron, $V_{pr}$ is the probe voltage, and $V_p$ is the plasma potential. From the electron current at the plasma potential ($I_{es}$: the ES current), one can readily obtain the electron density

$$I_{es} = n_e e A_p \left(\frac{kT_e}{2\pi m_e}\right)^{\frac{1}{2}}. \quad (2)$$

To accurately measure plasma parameters, the harmonic technique, which exploits the generation of harmonics resulting from excitation of the nonlinearity of the single Langmuir probe characteristics, combined with Druyvesteyn method was used.[3,4] In the harmonic method, the voltage applied to a probe consists of the sweep voltage and the sinusoidal voltage $v_0$ of the frequency $\omega$. The current was obtained by measuring the voltage difference across the sensing resistor (100 Ω) using the differential amplifier. After data processing in the analog-to-digital converter, the fast Fourier transform was performed to find the second harmonic of the I-V characteristic. The second harmonic term $I_{2\omega}$ of the measured probe current is proportional to the second derivative as $I_{2\omega} \approx (1/4)\, v_0^2\, (d^2I/dV^2) \cos 2\omega t$, which is related to the EEDF, $f(\epsilon)$,

$$f(\epsilon) = \frac{2m_e}{e^2 A_p} \left(\frac{2eV}{m_e}\right)^{1/2} \frac{d^2I}{dV^2}, \quad (3)$$

where $V$ is the probe potential referenced to $V_p$ and $\epsilon$ is measured in units of eV. The electron energy probability function (EEPF), $f_p(\epsilon)$, is related to the EEDF as, $f_p(\epsilon) = f(\epsilon)/\sqrt{\epsilon}$. The $n_e$ and the effective electron temperature ($T_{eff}$) are calculated with the measured EEDF as follows:

$$n_e = \int_0^{\epsilon_{max}} f(\epsilon) d\epsilon, \quad T_{eff} = \frac{2}{3n_e} \int_0^{\epsilon_{max}} \epsilon f(\epsilon) d\epsilon, \quad (4)$$

where $\epsilon_{max}$ is determined by the dynamic range of the EEDF measurement. The electron temperature can also be determined from the slope of the probe I-V curve in the exponential region (from the point where the probe current is zero to where the slope of the curve begins to decrease). We observed that both methods yield almost same values of the electron temperature. If the EEDF based on the harmonic method provides the most reliable and accurate way to determine the plasma parameters, there should not be any reason for the discrepancy between the ion density obtained from the probe I-V curve and the plasma density obtained from the EEDF integration method.

It has been known that the ion saturation current method may give rise to overestimated values of the plasma density compared with the electron current methods (the ES current method and the EEDF integration methods). The plasma density measured using the ion saturation current method can even be several orders of magnitude larger than the density measured using the ES and EEDF methods.[5] In Langmuir probe measurement, ion currents are much smaller than electron currents. An easy method to measure the ion saturation current is to obtain I-V data at a large negative voltage with respect to the plasma potential in order to minimize electron collection. In that case, expansion of the sheath around the probe can make the collection area much larger than the physical probe area. A conventional method of correcting the ion data is to linearly extrapolate the ion current measured at a large negative voltage region to that at the plasma potential. Fitting procedure over the large voltage range may lead to a significant error. However, if we properly apply the CL sheath formula for the sheath thickness of the probe at the floating potential, we can reduce the error of the ion current method.[11]

It has been found experimentally that ion saturation currents $I_i$ to cylindrical probes in the $10^{10}$–$10^{12}$ cm$^{-3}$ density range tend to follow an $I_i \propto (V_p - V_{pr})^{3/4}$(Child-Langmuir sheath law).[11] If we assume this, one can obtain an estimate of the positive ion current at the floating potential ($V_f$) by extrapolating to the floating potential. Since the sheath is well established at the floating potential, and the expected $I_i(V_f)$ can be calculated without the uncertainties inherent in extrapolating to the plasma potential due to the weak ion-accelerating fields there. The positive ion density can be evaluated also from the measured ion current at the floating potential ($I_i(V_f) \approx 0.5\, eA_f n_+ c_s$). Here, $A_f$ is the sheath area of a cylindrical probe at $V_f$, $n_+$ is the positive ion density, and $c_s = \sqrt{kT_e/m_+}$ is the normal Bohm speed at the sheath edge ($m_+$ is the ion mass). In order to know $A_f$, the sheath thickness ($d$) should be determined. The sheath thickness was estimated from the CL sheath law at the floating potential: $d = 1.018\, ((V_p - V_f)/kT_e)^{3/4} \lambda_D$ ($\lambda_D$ is the Debye length). Then, the positive ion density can be obtained as[11]

$$n_+ = \frac{I_i(V_f)}{0.5\, c_s\, 2\pi (r_p + d)\, l}, \quad (5)$$

where $l$ and $r_p$ are the length and radius of the electric probe.

To determine the positive ion density from another way, the OML ion current theory can be used for the low density

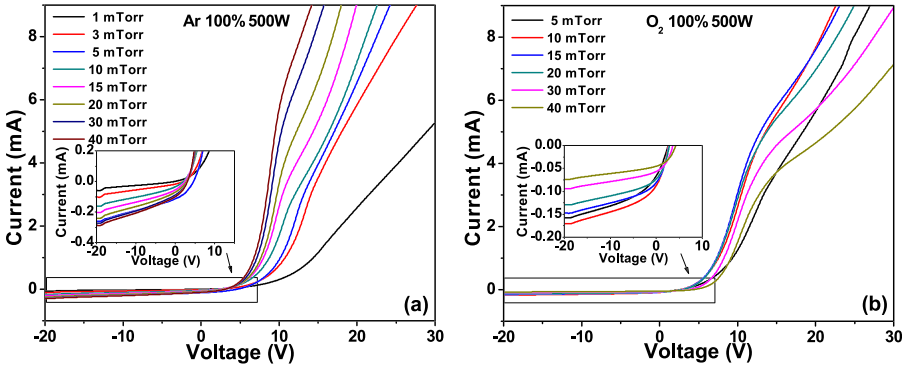


FIG. 1. (a) Measured probe current-voltage (I-V) characteristic curves for ICP Ar discharges at different pressures. (b) Measured probe current-voltage (I-V) characteristic curve for ICP $O_2$ discharges at different pressures. The insets exhibit the magnified graph of the probe current at the negatively biased probe voltages.

plasmas with thick sheath, and the positive ion current ($I_i$) is expressed as[17]

$$I_i = n_+ e A_p \left(\frac{kT_i}{2\pi m_+}\right)^{\frac{1}{2}} \frac{2}{\sqrt{\pi}} \left(1 - \frac{e(V_p - V_{pr})}{kT_i}\right)^{\frac{1}{2}}, \quad (6)$$

where $T_i$ is the ion temperature. In the positive ion saturation region where the probe current is virtually all positive ion current, we can plot $I_i^2 = AV_{pr} + B$ ($A$ and $B$ are constants). From the slope, we can determine the positive ion density. The OML result is very restricted in applicability. Since the sheath radius in OML theory was taken to be infinite, the density has to be so low that the sheath is much larger than the probe radius. Also, the collisionless OML theory holds when the mean free path $\lambda_i$ of ions and $\lambda_e$ of electrons are larger than $\lambda_D$ and $r_p$. It is worth noting that ions having the angular momentum larger than a specific value $(m_+(2E_0/m_+)^{1/2}\lambda_i$: $E_0$ is the initial energy of the ion) will not be collected by the probe and will be reflected to infinity. Therefore, the OML theory is not valid when the proportion of ions that encounter an absorption barrier is large. In principle, when the initial energy of the ion is small, the OML theory fails if[17]

$$\lambda_i < r_p \left(-\frac{e(V_p - V_{pr})}{kT_i}\right)^{\frac{1}{2}}. \quad (7)$$

In Ar plasmas, when $p = 4$ mTorr, $\lambda_i$ becomes about 3.8 mm, and when $p = 40$ mTorr, $\lambda_i$ is decreased to 0.85 mm. If we apply $|V_{pr} - V_p| = 30$ V and assume $T_i = 0.1$ eV, then the validity of the OML is fulfilled within the pressure range up to 30 mTorr since the small radius probe tip ($r_p = 0.1$ mm) is used in this work.

## III. RESULTS AND DISCUSSIONS

Figures 1(a) and 1(b) represent I-V traces taken by the electric probe for ICP Ar and $O_2$ discharges at different pressures, respectively. They retain typical I-V characteristics of the electric probe. We have analyzed these I-V curves to obtain the plasma parameters from various probe theories. Equation (6) predicts that a plot of $I_i^2$ versus $|V_{pr} - V_p|$ should be linear, as shown in Fig. 2(a). It is seen that the linear dependence in $I_i^2 - |V_{pr} - V_p|$ is following almost exactly at pressures 10–40 mTorr. As long as $I_i$ follows OML scaling, the value of $n_+$ obtained by OML theory is much more trustworthy than any value of $n_e$ derived from the electron saturation current.[8] However, it is noted that at the pressures 1 and 3 mTorr, the $I_i - |V_{pr} - V_p|$ characteristics were linear, rather than parabolic, which causes some uncertainty in the application of OML theory. Next, in order to obtain the sheath thickness at the floating potential, $d$, in Eq. (5) (based on the Child-Langmuir sheath model), the ion saturation region of the I-V characteristic curve is raised to the 4/3 power and plotted against $V_{pr}$, as shown in Fig. 2(b).

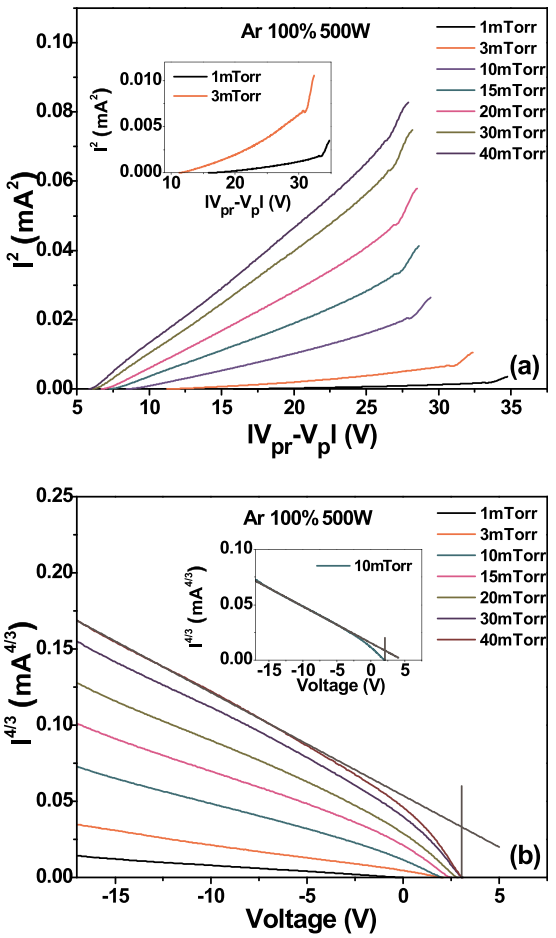


FIG. 2. (a) Measured ion current squared ($I_i^2$) vs the probe voltage ($V_{pr}$) referenced to the plasma potential ($V_p$) for Ar plasmas at different pressures. The inset represents the graphs for 1 and 3 mTorr. (b) Ion current $I_i^{4/3}$ vs $V_{pr}$ for Ar plasmas at different pressures, and a least-squares fitted straight line. The intersection of the line with the vertical line at floating potential $V_f$ yields the value of $I_i(V_f)$ used in the analysis. The inset shows the fitting and extrapolation for the 10 mTorr plasma.

A straight line is fitted to the part of the curve that is not affected by electron current. Extrapolating to $V_f$, where $I_i - I_e = 0$, gives an estimate of $I_i(V_f)$.

Figure 3 illustrates the variations of the plasma density in Ar ICP discharge at 500 W as a function of pressure. In accordance with the global modeling[18,19] and the previous experiments,[1,20] the plasma density increases with increasing pressure. The comparison is made on the plasma densities measured by different methods; the EEDF integration method ($n_e$ EEDF), the electron saturation current ($n_e$ ES), the ion current at the floating potential based on the Child-Langmuir sheath law ($n_i$ CL), and the orbital-motion-limited ion current ($n_i$ OML). As can be seen in the figure, there exist some differences between them. It is observed that the plasma density deduced from the OML method is larger than other three methods. This may be explained by the fact that the slope of $I_i^2 - |V_{pr} - V_p|$ curve is overestimated. The orbital ion motion is sensitive to ion collision in the sheath and orbital motion is destroyed at quite low pressure. The ion orbits were changed by collisions at low density, thus increasing the collected current. However, the OML method gives comparable densities to those obtained by other methods at pressure above 20 mTorr. This can be explained by the decrease in sheath thickness with increasing plasma density: not many collisions can occur in a thin sheath.[8] In a low pressure region, the CL sheath method gives much lower plasma density. This is attributable to the fact that the CL sheath formula applies to planes, not cylinders and the Debye sheath thickness has been neglected, as well as orbiting. Also, the CL sheath law in estimating $d$ is not applicable in low-$n_e$ region. These aspects become significant when the sheath thickness becomes large (i.e., at low pressure).

Figure 4 shows the comparison of the plasma densities obtained by various methods at different pressures in oxygen discharge. In this case, the plasma densities obtained by OML theory are comparable to those from the ion current at the floating potential. In oxygen discharges, we may well apply the OML theory because the plasma density is so low that the sheath can be considered to be much larger than the probe radius. It is observed that the difference between the OML and CL results is not severe and all the estimates are within error limit. The $n_e$ obtained by both the EEDF method

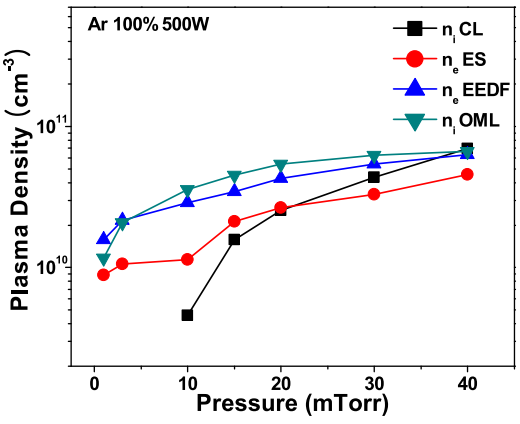


FIG. 3. Comparison of the plasma densities using the CL sheath method, EEDF method, OML, and ES current method in Ar ICP discharges.

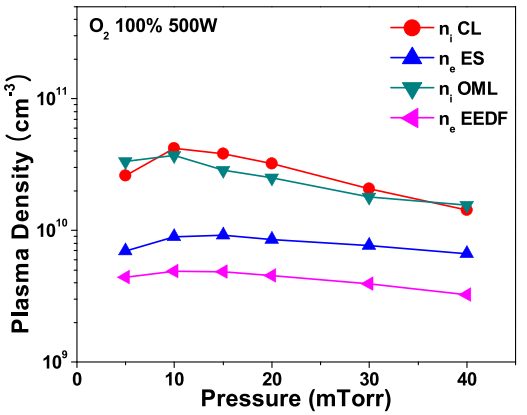


FIG. 4. Comparison of the electron densities obtained by the ES and EEDF methods, and the positive ion densities obtained by the OML and CL sheath methods in $O_2$ ICP discharges.

and the ES methods give values almost an order of magnitude less than the plasma density ($n_i$) measured by using the OML and CL sheath methods. The significant difference between the positive ion density and electron density is mainly attributable to the presence of negative ions in oxygen discharges. However, it should be noted that the probe technique has some limitation for the oxygen discharges because the interpretation of the probe I-V characteristic is complicated in electronegative plasmas. As is inferred from the inset of Fig. 1(b), a clear linear dependence in the $I_i^2 - |V_{pr} - V_p|$ curve has not been observed for the oxygen discharges. Therefore, the positive ion densities obtained from the OML and CL sheath methods may have larger error bounds due to the uncertainties associated with the slope in $I_i^2 - |V_{pr} - V_p|$ curve and with the floating potential. The contribution from negative ions may cause a steeper slope of the curve (especially in the region of small $|V_{pr} - V_p|$), which may lead to the overestimation of the positive ion density deduced from the OML theory. Relatively low $n_e$ in the oxygen discharges may hinder the validity of the CL sheath law. The presence of negative ions may also prevent a precise determination of the positive ion current at the floating potential, which may lead to the overestimated $I_i(V_f)$. Therefore, it would be difficult to assert that the difference in Fig. 4 between the positive ion and electron densities is the negative ion density. To better estimate the negative ion density, some authors suggested alternative approaches utilizing a comparison of the experimental I-V curve with the theoretical model of the positive ion flux.[21–23]

The plasma density deduced from the EEDF methods only reflects the electron populations with all energies. On the other hand, the ES current contains the contribution from the negative ions. This might be a reason why the $n_e$ obtained by the ES method is larger than that obtained by the EEDF method. As shown, in $O_2$ plasmas, the electron density (obtained by the EEDF method) varies weakly with pressure compared to Ar plasmas over the range studied.[24] The plasma density is observed to increase with increasing pressure at a low-pressure range, and have a maximum, and then decreases slightly. This behavior was also observed in our earlier works.[25–27] This behavior seems to be related to the

transition of the dominant loss mechanism of charged particles in electronegative plasmas. At a low pressure range, the dominant loss of charged particles is due to diffusion, while as the pressure is increased, the loss channel via the volume recombination is added. The increase of recombination loss along with the diffusion loss makes the charged particle density decrease. In addition to this effect, a decrease in the ionization rate with increasing pressure through the decrease of the electron temperature can contribute to the transition. A similar variation was observed in an experiment with a sophisticated correction of the probe I-V data.[28]

The EEPF is one of the most important plasma characteristics as it dominates all electron-impact processes.[24] Electrons with sufficiently large kinetic energy can overcome the potential difference between the plasma and the chamber walls and escape to the walls. The deviation of measured EEPFs from an otherwise Maxwell-Boltzmann form is often attributed to a depletion of the high-energy tail region by either this mechanism or by inelastic electron-atom collisions.[29] The wall loss of electrons produces a distinct steep drop in the EEDF at electron energies higher than the wall potential energy.

Figure 5 represents the evolutions of the EEPFs in Ar discharges with increasing pressures (at the ICP power of 500 W). It has been reported that collisionless stochastic heating characterized by a bi-Maxwellian-type EEDF dominates in an ICP discharge operating at low gas pressure.[30,31] But such a bi-Maxwellian distribution is not observed in this study. This can be explained on the basis of comparison between the electron residence time and the electron-electron collision time.[32] Above moderate ICP powers, the plasma density becomes high enough $(n_e \approx 10^{11}\text{cm}^{-3})$ so that the electron-electron collision becomes effective. If the electron-electron collision time is less than the electron residence time, an electron will collide with other electrons at least one time, resulting in the occurrence of electron energy thermalization. As the pressure increases, the increased discharge current enhances the Ohmic heating of low-energy electrons in the bulk. This results in the shift of EEPF to Maxwellian distribution. Therefore, at high gas pressure, collisional Ohmic heating in the plasma bulk dominates, being characterized by Maxwellian or Druyvesteyn-type EEDF (due to a higher depletion in the high-energy tail as the pressure increases).[33] However, in this work, the EEPFs measured in low-pressure Ar plasmas are obviously Maxwellian as shown in the figure. At low pressure such as 1 mTorr, a depletion of the electron population is observed above 15 eV due to ionization collision and loss to the chamber walls. But, as the pressure is increased, fast electrons are moderated by neutrals and the depletion is observed around the excitation energy of argon (11.55 eV). This behavior holds until the pressure is increased to 10 mTorr and the depletion occurs at lower electron energies for the pressures above that. Even though the measured EEPFs exhibit a slight depletion in the high-energy tail as the pressure increases, they are observed to remain close to Maxwellian. Note the presence of a well reproduced Maxwellian distribution in the low-energy part of the EEPFs at relatively high Ar pressure, where the plasma density is sufficiently large to provide a strong Maxwellizing effect due to electron-electron collisions.[34,35]

Figure 6 illustrates the evolutions of the EEPFs in oxygen discharges with increasing pressures (at the ICP power of 500 W). The high-energy tails of the EEDFs are also observed to be less populated, as a result of a higher global cross section in oxygen.[36] The EEPFs exhibit a rapid change with pressure due to many molecular collision processes. Depleted electrons at certain electron energies in the EEPF indicate various collision processes, such as ionization and excitation, including vibration and rotation collisions, as well as the escaping electrons to the chamber walls. Because the electron-$O_2$ collision cross sections for excitation, dissociative attachment, and some modes of vibrational collisions (most of vibrational collisions have high cross sections at 0.1–3 eV) have threshold around 5 eV,[37] the EEPF develops different temperature structures at low energies, intermediate energies, and tail energies responsible for the ionization in the plasma.[38,39] The depletion occurs at much less electron energies compared to the argon discharges. This is caused by opening various electron energy loss channels mentioned above. Since the electron density is so low in the oxygen discharges that electron-neutral collision is dominant and the EEPF becomes deviated slightly from Maxwellian distribution at low-electron energy region. Especially, the EEPF appears to change from a single temperature Maxwellian to a two temperature shape with increase in pressure above 15 mTorr,

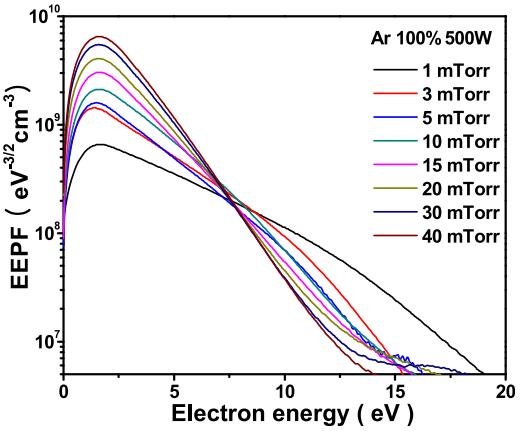


FIG. 5. EEPFs for Ar ICP discharges at different pressures.

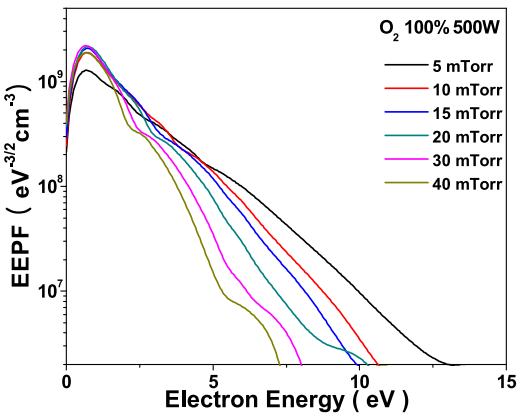


FIG. 6. EEPFs for $O_2$ ICP discharges at different pressures.

accompanied by a significant depletion of the high-energy tail. Similar structure in the EEPF has been observed by Gudmundsson and Lieberman.[40,41]

## IV. CONCLUSIONS

The plasma densities were obtained by using different ways to interpret the probe current-voltage curve and compared. The results indicate that even though the OML method gives a little overestimated plasma densities, there exists overall good agreement between the plasma densities determined by various interpretation methods. Especially, in low-pressure oxygen discharges, a determination of plasma density based on OML theory gives a fair estimate of the plasma density and compares well with the CL sheath method. We found that the harmonic method (the ac superimposed method) provides reasonable estimate of plasma parameters. Considering inherent uncertainties associated with electric probes, these interpretation methods do not produce significant errors in the parameter region of this work. The EEPF in Ar plasmas was observed to be obviously Maxwellian. Although the EEPFs in $O_2$ discharges appeared to change from a single temperature Maxwellian to a two temperature shape with increase in the pressure above 15 mTorr, accompanied by a significant depletion of the high-energy tail, the EEPFs were nearly Maxwellian at the range of the operating pressure 1–40 mTorr. Thus, the assumption of Maxwellian energy distribution in Ar and $O_2$ ICP plasmas in pressures between 1 and 40 mTorr gives a fairly accurate determination of the $n_e$ and $T_e$ based on various interpretation methods of the probe I-V data.

## ACKNOWLEDGMENTS

Helpful discussions with Professor K. S. Chung, Professor C. W. Chung, and Dr. H. C. Lee of Hanyang University are greatly acknowledged. This work was supported by the National Research Foundation of Korea (NRF) funded by the Ministry of Education, Science and Technology (Grant No. 20120005928, Fusion Core Research Center Program).

[1]T. H. Chung, H. R. Kang, and M. K. Bae, Phys. Plasmas **19**, 113502 (2012).
[2]V. A. Godyak, R. B. Piejak, and B. A. Alexandrovich, Plasma Sources Sci. Technol. **1**, 36 (1992).
[3]S.-H. Seo, C.-W. Chung, J.-I. Hong, and H.-Y. Chang, Phys. Rev. E **62**, 7155 (2000).
[4]J. Y. Bang, A. Kim, and C. W. Chung, Phys. Plasmas **17**, 064502 (2010).
[5]J. L. Jauberteau and I. Jauberteau, Plasma Sources Sci. Technol. **17**, 015019 (2008).
[6]V. A. Godyak and V. I. Demidov, J. Phys. D: Appl. Phys. **44**, 233001 (2011).
[7]V. Pletnev and J. G. Laframboise, Phys. Plasmas **13**, 073503 (2006).
[8]F. F. Chen, Plasma Sources Sci. Technol. **18**, 035012 (2009).
[9]L. S. Pilling and D. A. Carnegie, Plasma Sources Sci. Technol. **16**, 570 (2007).
[10]F. F. Chen, Phys. Plasmas **8**, 3029 (2001).
[11]F. F. Chen, J. D. Evans, and D. Arnush, Phys. Plasmas **9**, 1449 (2002).
[12]D. L. Flamm, Plasma Chem. Plasma Process. **1**, 37 (1981).
[13]A. Granier, F. Nicolazo, C. Vall'ee, A. Goullet, G. Turban, and B. Grolleau, Plasma Sources Sci. Technol. **6**, 147 (1997).
[14]T. Sato and T. Makabe, J. Appl. Phys. **98**, 113304 (2005).
[15]Y. Hayashi, S. Hirao, Y. Zhang, T. Gans, D. O'Connell, Z. Lj. Petrovic, and T. Makabe, J. Phys. D: Appl. Phys. **42**, 145206 (2009).
[16]M. A. Song, Y. W. Lee, and T. H. Chung, Phys. Plasmas **18**, 023504 (2011).
[17]J. E. Allen, Phys. Scr. **45**, 497 (1992).
[18]J. T. Gudmundsson and E. G. Thorsteinsson, Plasma Sources Sci. Technol. **16**, 399 (2007).
[19]E. G. Thorsteinsson and J. T. Gudmundsson, Plasma Sources Sci. Technol. **18**, 045001 (2009).
[20]M.-H. Lee, S.-H. Jang, and C.-W. Chung, J. Appl. Phys. **101**, 033305 (2007).
[21]R. Morales Crespo, J. I. Fernandez Palop, M. A. Hernandez, S. Borrego del Pino, and J. Ballesteros, J. Appl. Phys. **96**, 4777 (2004).
[22]P. Chabert, T. E. Sheridan, R. W. Boswell, and J. Perrins, Plasma Sources Sci. Technol. **8**, 561 (1999).
[23]T. E. Sheridan, P. Chabert, and R. W. Boswell, Plasma Sources Sci. Technol. **8**, 457 (1999).
[24]C. C. Hsu, M. A. Nierode, J. W. Coburn, and D. B. Graves, J. Phys. D: Appl. Phys. **39**, 3272 (2006).
[25]T. H. Chung, D. C. Seo, and H. J. Yoon, J. Appl. Phys. **86**, 3536 (1999).
[26]D. C. Seo, T. H. Chung, H. J. Yoon, and G. H. Kim, J. Appl. Phys. **89**, 4218 (2001).
[27]D. C. Seo and T. H. Chung, J. Phys. D: Appl. Phys. **34**, 2854 (2001).
[28]P. Bryant, A. Dyson, and J. E. Allen, J. Phys. D: Appl. Phys. **34**, 95 (2001).
[29]A. Meige and R. W. Boswell, Phys. Plasmas **13**, 092104 (2006).
[30]S. H. Seo, J. I. Hong, and H. Y. Chang, Appl. Phys. Lett. **74**, 2776 (1999).
[31]H.-C. Lee, M.-H. Lee, and C.-W. Chung, Phys. Plasmas **17**, 013501 (2010).
[32]H.-C. Lee, J.-K. Lee, and C.-W. Chung, Phys. Plasmas **17**, 033506 (2010).
[33]E. Abdel-Fattah, M. Bazavan, and H. Sugai, J. Appl. Phys. **110**, 113303 (2011).
[34]H.-C. Lee, A. Kim, S. Y. Moon, and C.-W. Chung, Phys. Plasmas **18**, 023501 (2011).
[35]C.-M. Tsai, A. P. Lee, and C. S. Kou, J. Phys. D: Appl. Phys. **39**, 3821 (2006).
[36]K. Kutasi, V. Guerra, and P. A. Sa, J. Phys. D: Appl. Phys. **43**, 175201 (2010).
[37]D. Benyoucef, M. Yousfi, and B. Belmadani, J. Appl. Phys. **109**, 083304 (2011).
[38]H. Singh and D. B. Graves, J. Appl. Phys. **87**, 4098 (2000).
[39]H. Singh and D. B. Graves, J. Appl. Phys. **88**, 3889 (2000).
[40]J. T. Gudmundsson and M. A. Lieberman, Plasma Sources Sci. Technol. **7**, 1 (1998).
[41]S. V. Singh, J. Appl. Phys. **103**, 083303 (2008).